(1)161—168

第19卷第3期
2000年6月

红外与毫米波学报
J. Infrared Millim. Waves

Vol. 19, No. 3
June, 2000

# NOVEL HOMOJUNCTION FAR INFRARED DETECTORS*

SHEN Wen-Zhong[1,2]

([1]Department of Applied Physics, Shanghai Jiao Tong University, Shanghai 200030, China**;
[2]National Laboratory for Infrared Physics, Shanghai Institute of Technical Physics,
Chinese Academy of Sciences, Shanghai 200083, China)

**Abstract** The recent development of p-GaAs and Si homojunction interfacial workfunction internal photoemission (HIWIP) far-infrared (>40$\mu$m) detectors was briefly reviewed, both theoretically and experimentally. The emphasis is on the detector photoresponse mechanism and detector performance. Promising results indicate that p-GaAs and Si HIWIP far-infrared detectors have great potentiality to become a strong competitor in far-infrared applications.

**Key words** homojumotion structures, far-infrared, detectors.

# 新型同质结构远红外探测器*

沈文忠[1,2]

([1]上海交通大学应用物理系，上海，200030**；
[2]中国科学院上海技术物理研究所红外物理国家重点实验室，上海，200083)

TN215

**摘要** 从理论和实验两方面简要评述了p-GaAs和Si同质结界面功函数内光发射(HIWIP)远红外(>40$\mu$m)探测器的最新发展.重点讨论了此探测器的光响应机制和探测器性能.结果表明，p-GaAs和Si的HIWIP远红外探测器有希望成为远红外应用中具有强大竞争力的器件.

**关键词** 同质结构，远红外，探测器.

## INTRODUCTION

Semiconductor photodetectors are the most sensitive detectors of infrared radiation. Progress in the crystalline quality of materials, the control of unwanted impurities and the fabrication of contacts have produced increasingly sensitive and stable detectors. These improvements were due in part to parallel developments of semiconductor industry, as well as the demands and potentiality of infrared astronomy programs, such as Space Infrared Telescope Facility (SIRTF) and Far Infrared and Submillimeter Telescope (FIRST). According to the mechanism of photoexcited processes, semiconductor infrared detectors can be described mainly as intrinsic and extrinsic detectors. The cutoff wavelength ($\lambda_c$) of intrinsic detectors is determined by their band gap, while the $\lambda_c$ of extrinsic detectors is determined by the impurity photoionization energy. Figure 1 shows the cutoff wavelengh of several semiconductor intrinsic and extrinsic detectors. The horizontal line represents the detector's extended coverage of cutoff wavelength by using alloying or uniaxial stress. Si-based blocked impurity band(BIB) detectors have become the state of the art for infrared detection in the 15-40$\mu$m. Si:As BIB arrays, which cover the wavelength from 5 to 28$\mu$m, can be obtained in 256×256

* This work was supported in part by the Foundation of Education Administration for Excellent Young Teachers and the National Natural Science Foundation of China (No. 69606006).
** Mailing address
Received 1999-10-05

* 部分得到国家教育部优秀青年教师教学与科研奖励基金和国家自然科学基金(编号69606006)资助
** 通讯地址
稿件收到日期 1999-10-05

array format. Recently, Huffman *et al.* have developed the material for Si:Sb BIB arrays, which extends the wavelength detection to 40μm[1]. Beyond 40μm, Ge:Ga is the most common photoconductor material with a cutoff wavelength of ~100μm. The uniaxial compression approach takes advantage of the decrease in binding energy of shallow acceptors, which results from splitting of the heavy hole and light hole valence band degeneracy and has extended the optical response of Ge:Ga to ~220μm. Most recently, stressed Ge:Ga has been utilized in a 5×5 detector array[2].

One of the primary goals of infrared detector development is to extend the wavelength coverage, in order to increase sensitivity in regions of spectrum that were previously covered by bolometric detectors. The far infrared and submillimeter range generally refers to the electromagnetic band from 30 to 1000μm and is the source of much astrophysical information, corresponding to the blackbody radiation for relatively cool object of 5-50K, as well as molecular and atomic emission lines associated with important species such as C, O, $H_2O$. Dust, which is present both around and between stars, absorbs higher energy photos, causing stars and galaxies to emit significant radiation in the far infrared, too. Nevertheless, there are many technological challenges for fabricating large format arrays in germanium[3]. Incorporating different components in a single chip to fabricate an integrated circuit is a major advantage of using Si. Furthermore, the recent rapid development of GaAs based long wavelength quantum well infrared photodetectors (QWIPs) and focal plane array cameras[4] makes GaAs another promising candidate for integrated circuits. In this paper, a novel far infrared detection is proposed to extend the wavelength coverage by use of the concept of internal photoemission and has been realized in GaAs and Si homojunction structures.

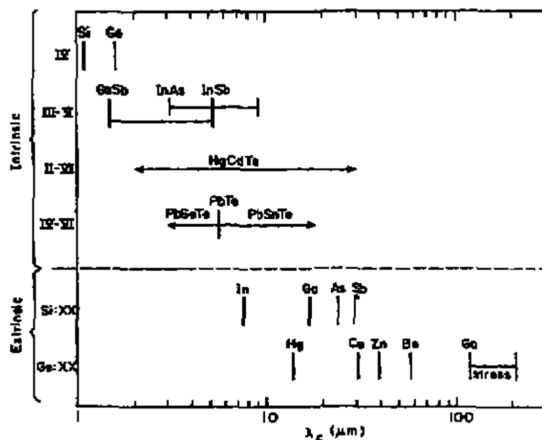


Fig. 1 Cutoff wavelength of several semiconductor intrinsic and extrinsic detectors. The horizontal line represents the detector's extended coverage of cutoff wavelength by using alloying or uniaxial stress

图1 几种本征和非本征半导体探测器的截止波长

## 1 DETECTION MECHANISM

The basic structure of homojunction internal photoemission (HIP) detectors consists of a heavily doped layer, which acts as the IR absorber region, and an undoped intrinsic layer across which most of

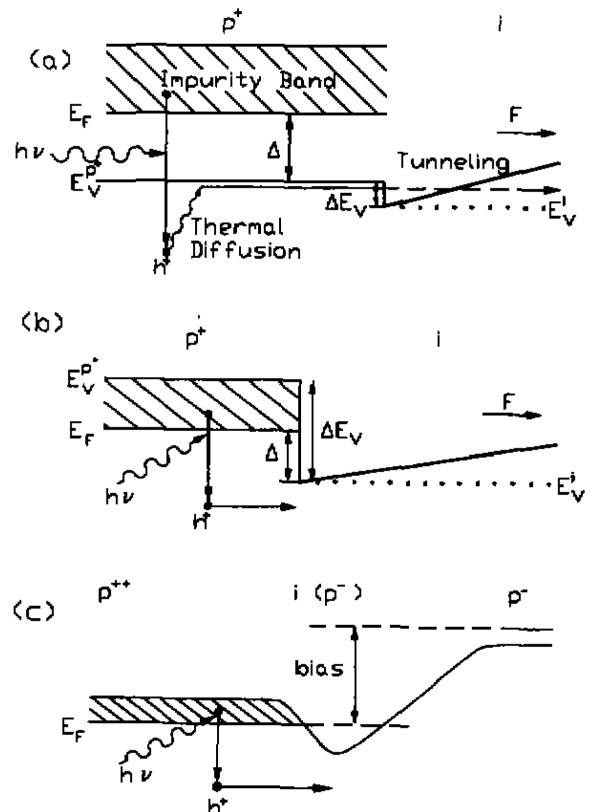


Fig. 2 Energy band diagrams for three different p types of HIP detectors. (a) Type Ⅰ: $N_a<N_c$; (b) Type Ⅱ: $N_c<N_a<N_0$; (c) Type Ⅲ: $N_a>N_0$. ($N_c$ is the Mott's critical concentration, $N_0$ is the critical concentration corresponding to $\Delta=0$)

图2 3种不同p型同质结内发射探测器的能带图

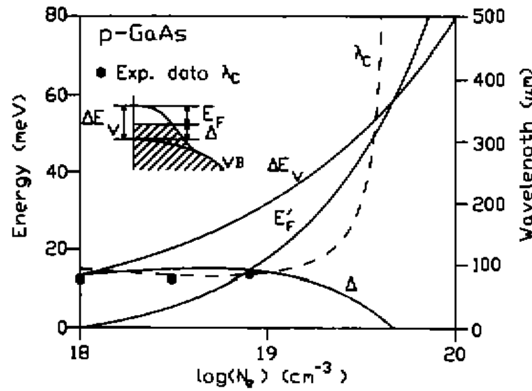


Fig. 3 Calculated emitter layer doping concentration ($N_e$) dependence of the shift for the major band edge $\Delta E_v$ and interfacial work function $\Delta$ at zero bias from the high density (HD) theory. The theoretical curve of $\Delta$ should have a deviation of $\pm$1meV due to the modified Fermi level. The experimental HIWIP cutoff wavelength results are shown by solid circles

图 3　不同发射层掺杂浓度下能带移动的理论计算值

the external bias is dropped. According to the doping concentration level in the heavily doped layer, the HIP detectors can be divided into three types as shown in Figs 2 (a)～(c), which show different photoresponse mechanisms and response wavelength ranges.

When the doping concentration ($N_a$) in the $p^+$-layer is high but below the Mott critical value ($N_c$), an impurity band is formed. At low temperatures, the Fermi level is located in the impurity band. The incident FIR radiation is absorbed due to the impurity photoionization, with a workfunction (or cutoff wavelength) given by $\Delta = E_F - E_v^{p^+}$. The operation can be described as follows. Holes are photoexcited from filled impurity band states and rapidly thermalized into the top of the valence band by phonon relaxation and then tunnel through an interfacial barrier. The cutoff wavelength is mainly determined by impurity photoionization energy.

When the doping concentration is above the Mott transition, the impurity band is linked with the valence band edge, and the $p^+$-layer becomes metallic. Even in this case, the Fermi level can still be above the valence band edge of the i-layer ($E_F > E_V'$) due to the bandgap narrowing effect, giving rise to a workfunction $\Delta = E_F - E_v^i$ as shown in Fig. 2(b), unless $N_a$ exceeds a critical concentration $N_0$ at which $\Delta = 0$. One of their unique features is that in principle, there is no restriction on $\lambda_c$, which is tailorable, since the workfunction can become arbitrarily small with increasing doping concentration. This means that the HIWIP FIR detectors with any $\lambda_c$ can be developed as needed. Here, the photon absorption is due to free carrier absorption. By using high density theory[5], the doping concentration dependence of $\Delta E_v$, $E_F$, $\Delta$, and $\lambda_c$ was calculated. The results for p type GaAs

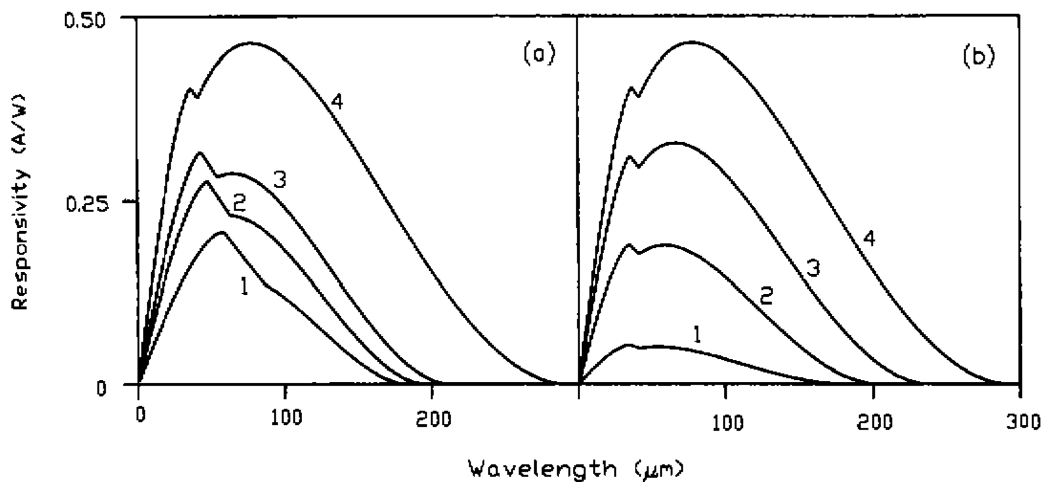


Fig. 4 (a) Spectral response calculated for four p-GaAs single layer detectors with the same electric field $F$ of 1000 V/cm but different emitter layer doping concentrations $N_e$: (1) $N_e = 5.0\times10^{18}\text{cm}^{-3}$; (2) $N_e = 8.0\times10^{18}\text{cm}^{-3}$; (3) $N_e = 1.0\times10^{19}\text{cm}^{-3}$; (4) $N_e = 1.5\times10^{19}\text{cm}^{-3}$. (b) The effect of electric field on spectral response is also shown for detector 4: (1) $F$=50V/cm; (2) $F$=200V/cm; (3) $F$=500V/cm; (4) $F$=1000V/cm

图 4　P-GaAs 单层探测器在不同掺杂浓度(a)和不同电场强度(b)下的波谱响应理论值

are shown in Fig. 3, together with our experimental HIWIP cutoff wavelength results by solid circles[6]. It is seen from Fig. 3 that the experimental $\lambda_c$ is in reasonable agreement with the calculation, and $\lambda_c$ becomes very sensitive to $N_a$ at high doping concentrations, that is, only a small increase in $N_a$ can cause a large increase in $\lambda_c$. Furthermore, $\lambda_c$ of the HIWIP detector can easily be tuned by the doping concentration to meet the requirements of 200μm or more. This type is our interest here.

When the doping concentration is so high that the Fermi level is below the valence band edge of the i-layer, the $p^+$-layer becomes degenerate, and a barrier associated with a space charge region is formed at the $p^+$-i interface due to the hole diffusion, as shown in Fig. 2(c). This type of device was first demonstrated by Tohyama *et al.* [7] The major difference is that it is expected to operate near 77K and has responses in the midwave infrared (MWIR) and long wave IR ranges.

## 2 THEORETICAL MODEL OF SPECTRAL RESPONSE

The total quantum efficiency is the product of photon absorption probability, internal quantum efficiency and barrier collection efficiency. By using their analytic expressions, the responsivity for GaAs $p^+$-i single structures has been calculated as functions of wavelength, electric field, emitter layer doping concentration, etc. The effect of emitter layer doping concentration on spectral response is shown in Fig. 4 (a). It can be seen that with the increase of doping concentration, both the spectral bandwidth and the peak responsivity ($R_p$) increase, while the short wavelength side of the spectral response almost remains the same. It is noted that the spectra do not

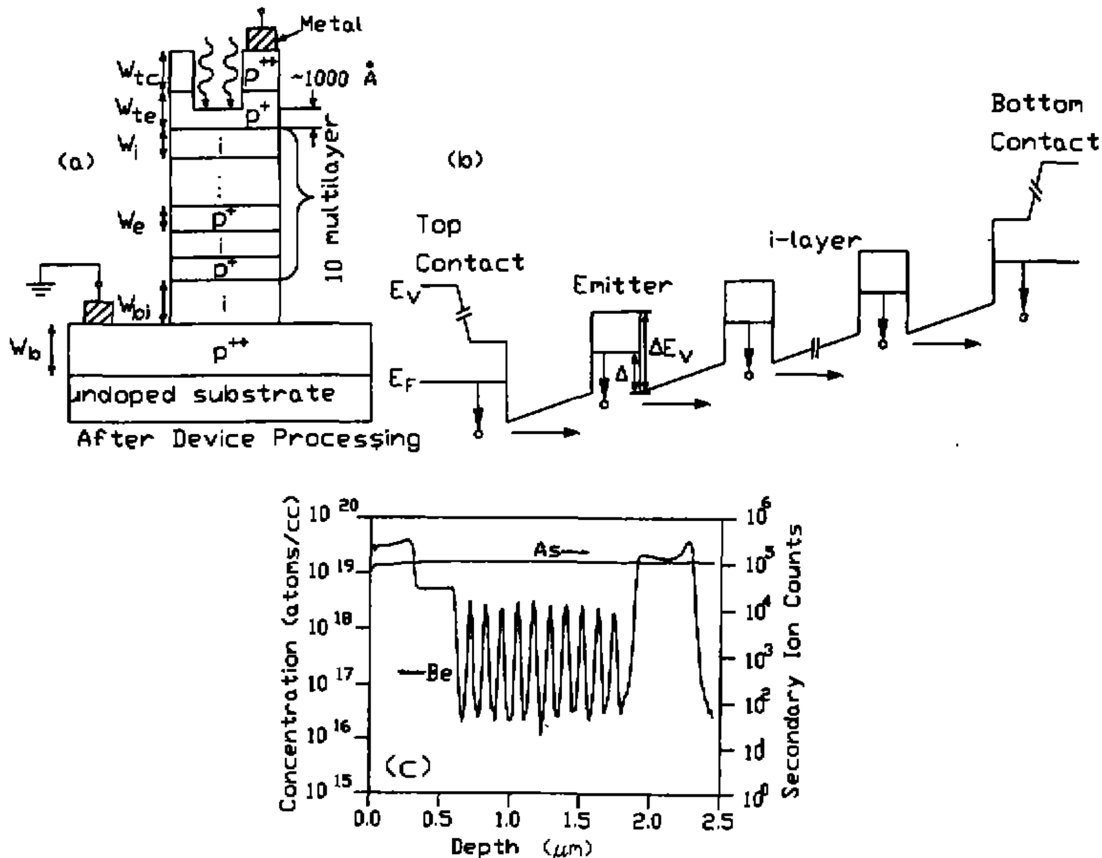


Fig. 5 (a) Schematic of 10-layer p-type HIWIP detectors after device processing. $p^{++}$, $p^+$ and i are the contact layer, emitter layer and undoped layer, respectively. A window is opened on the top side for frontside illumination. (b) Energy-band diagram of the detectors under forward bias. (c) SIMS profile of a Be doped p-GaAs HIWIP 10-layer detector sample

图5 器件处理后10层HINIP探测器的结构图(a),正向偏压下的能带图(b)和二次离子质谱(c)

change continuously at low wavelength range, because in that photon energy range the internal quantum efficiency has different function relations with photon energy. The corresponding $R_p$, $\lambda_c$, and $\Delta\lambda$ (half-peak width) are: $R_p$ = 0.20, 0.28, 0.32, and 0.47 A/W, $\lambda_c$ = 180. 194, 209, and 287μm, and $\Delta\lambda$ = 92, 96, 113, and 160μm. The calculated $R_p$ is in good agreement with the experimental results shown next by taking into account the multilayer effects. The electric field ($F$) dependence of spectral response is shown in Fig. 4 (b). As $F$ increases, both responsivity and $\lambda_c$ increase considerably due to the image force effect, which is in good agreement with experimental results below. Also, the peak wavelength shifts gradually to longer wavelengths. One important point to remember here is that the calculations are done for a single layer device. By using multilayer structures ($p^+$-i-$p^+$-i... or $n^+$-i-$n^+$-i...) and optimum emitter layer thickness, which can be realized by MBE or MOCVD growth technologies, the quantum efficiency can be easily improved, as shown experimenttally below.

## 3 EXPERIMENTAL RESULTS

The basic structure of HIWIP detectors consists of a heavily doped emitter layer and an intrinsic layer, across which most of the external bias is dropped. The detection mechanism involves infrared absorption in the emitter layer followed by the internal photoemission of photoexcited carriers across the junction barrier and then collection. The schematic of the detectors after device processing and their energy-band diagram are shown in Figs. 5a, 5b. Multilayers were used to increase the quantum efficiency due to the increased photon absorption efficiency and possible photocurrent gain enhancement. Good control of MBE growth is indicated by secondary ion mass spectroscopy (SIMS) measurements as shown in Fig. 5(c). The contact was formed by deposition of Ti-Pt-Au.

The MBE epilayers of our best p-GaAs HIWIP FIR detector consist of a 3000 Å bottom contact ($p^{++}$) layer, a 1500 Å undoped (i) layer, 20 periods of thin emitter ($p^+$) layers (thickness 150 Å) and undoped i layers (thickness 800 Å), and finally a 3000 Å top emitter layer and a 3000 Å top contact layer. The emitter layers were doped with Be to $4\times10^{18}cm^{-3}$. The top and bottom contact layers were doped to $2-3\times10^{19}cm^{-3}$, far above the Mott transition value to ensure an ohmic contact. The responsivity ($R$) spectra of the p-GaAs HIWIP FIR detector (mesa size 240μm×240μm) under different forward biases at 4.2K are shown in Fig. 6(a). The responsivities are greater than the previous results as this structure has 20 layers. The highest responsivity obtained here is 3.10A/W at a bias of 192.0mV. Figure 6(b) shows the bias dependence of the detectivity ($D^*$) and peak quantum efficiency $\eta_p$. The highest detectivity is $5.9\times10^{10}cmHz^{1/2}/W$ at 4.2K under a bias of 83.0mV. The maximum quantum efficiency in HIWIP FIR detectors can be estimated by taking into account the free carrier absorption and inelastic scattering loss. We get maximum quantum efficiency of 12.7% in the present GaAs detector, in good agreement with the experimental result of 12.5% at a bias of 192.0mV[8]. Two other detector samples with 10 layers and a single layer were also measured, with all the other parameters the same, and the maximum quantum efficiency was 6.1% and 0.5%, respectively, consistent with the theoretical prediction of 6.6% and 0.6%. The responsivity curves shown in Fig. 6 (a) also display a strong bias dependence of cutoff wavelength, increasing with the applied bias due to the image force effect. The experimental data are shown as solid circles in Fig. 6(c). The theoretical $\lambda_c$ (solid curve) is calculated and is in good agreement with the experimental results with a maximum deviation of 1.0meV.

The uniformity of the detectors was also tested[8]. The dark current of 7 randomly chosen relatively large mesas (460μm×460μm) at 4.2K was quite uniform (as shown in the inset of Fig. 7) with a standard deviation of 15.4% at a bias voltage of 200mV. Furthermore, the bias dependence of $D^*$ for the 7 mesas with a standard deviation of about 8.0% is shown in Fig. 7, the values are within experimental errors. These results clearly demonstrate the possibility of high uniformity required for large FIR focal

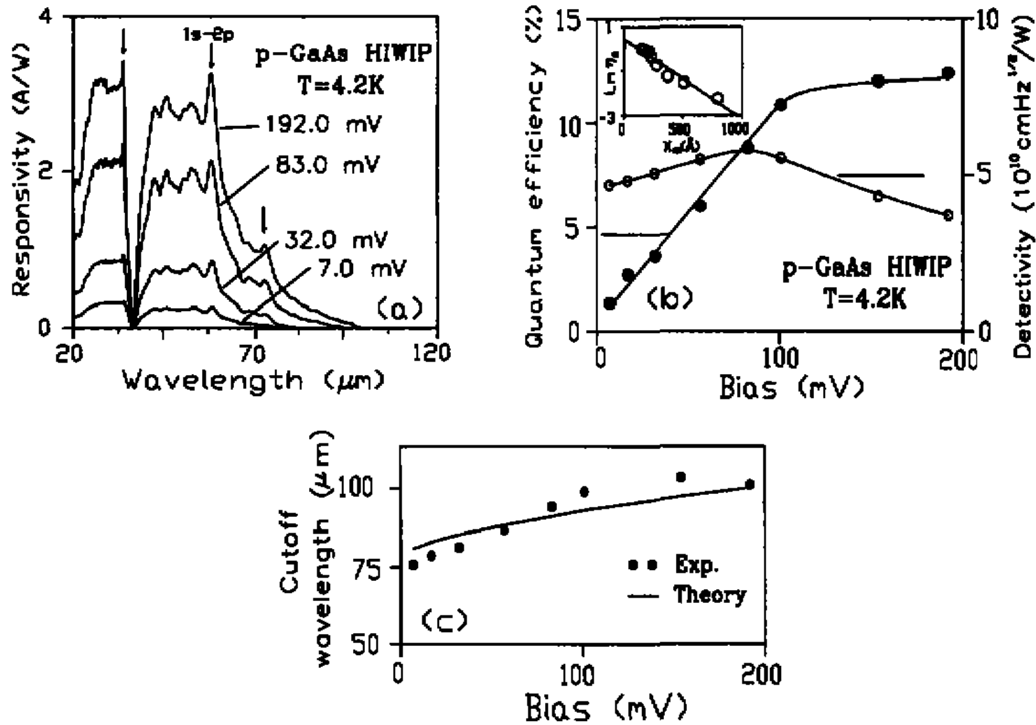


Fig. 6 (a) Spectral response of a 20-layer p-GaAs HIWIP FIR detector measured at 4. 2K under different forward bais values. The deep valley at 36. 5μm is due to the transverse optical (TO) phonons of GaAs. (b) Bias dependence of peak quantum efficiency measured at 30. 0μm (filled circles) and device detectivity (open circles). (c) Bias dependence of cutoff wavelength in the p-GaAs HIWIP detector at 4. 2K. The maximum deviation between the theory (solid curve) and experiment (filled circles) is 1. 0meV

图6 20层P-GaAs HIWIP远红外探测器的波谱响应(a),不同偏压下的量子效率及探测率(b),不同偏压下的截止波长(c)

plane arrays, since the typical pixel size for arrays is much smaller than the tested devices, (e. g., 50μm

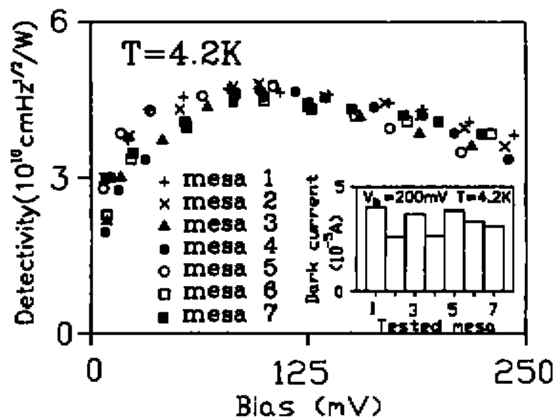


Fig. 7 Bias dependence of device detectivity of 7 randomly chosen 460μm-square mesas at temperature of 4. 2K. Shown in the inset is the dark current of the 7 mesas at 4. 2K and a forward bias of 200mV

图7 7个任选的探测器的探测率,插图为其200mV正向偏压下的暗电流

× 50μm in GaAs/AlGaAs QWIPs[4], and thus the dark current per pixel, together with the standard deviation, would be about two orders of magnitude smaller. Figure 8 shows the crosstalk of the p-GaAs HIWIP FIR detector measured by focusing the incident light spot on one mesa and monitoring the phtoconductivity outputs of the adjacent mesas. Output photoconductivity signal when the light is on mesas (a) and (b) (size 460μm square) as a percentage of direct incident signal. At the bias (83. 0mV), with the highest detectivity, the crosstalk is found to be 2. 29% for measa (a) and 0. 061% for mesa (b). The maximum output percentage (5. 70% and 0. 16%) corresponds approximately to the maximum output of the device at 192. 0mV. Lower values of crosstalk have been achieved under various bias conditions. This crosstalk is comparable to 2. 1% (in the first nearest column case) in Si:As BIB detectors[9].

Typical current noise spectra[10] of the studied p-

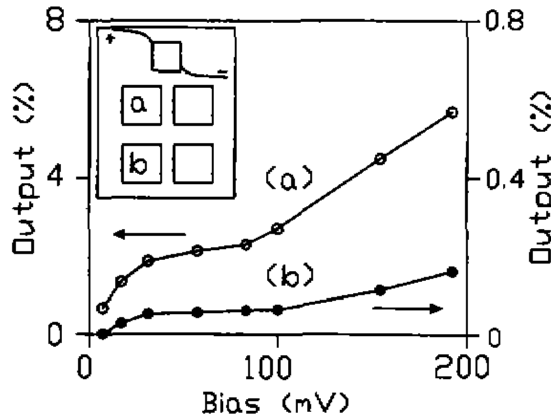


Fig. 8 The crosstalk of p-GaAs HIWIP measured by focusing the incident light spot on one mesa and monitoring the photoconductivity outputs of the adjacent mesas. Output photoconductivity signal when the light is on mesas a) and b) as a percentage of direct incident signal

图 8　p-GaAs HIWIP 远红外探测器的串音测量

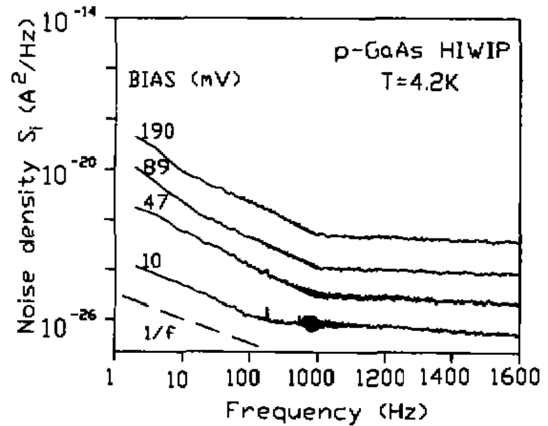


Fig. 9 Measured dark current noise spectra of p-GaAs HIWIP far-infrared detector at 4.2K for various forward biases. The dashed line represents the $1/f$ dependence of the noise power density $S_i$

图 9　正向偏压下探测器的暗电流噪声谱

GaAs HIWIP FIR detector at 4.2K for various forward bias values are presented in Fig. 9. All the spectra display 1/f noise dependence at frequencies ($f$) below 1kHz and are independent of frequency at higher values. The measured shot noise data can be used to directly estimate the noise equivalent power ($NEP$) in the p-GaAs HIWIP FIR detector. At a bias of 89mV, the measured shot noise ($S_i$) is $8.3\times10^{-25}A^2/Hz$, and the responsivity of the detector is 2.12A/W. This yields a $NEP$ of $4.3\times10^{-13}W/Hz^{1/2}$ (detectivity $D^*$ of $6.0\times10^{10}cmHz^{1/2}W$), also in good agreement with the previous optical estimation $D^*$ of $5.9\times10^{10}cmHz^{1/2}W$ at a bias of 83mV.

P-Si HIWIP FIR detectors have also been demonstrated[11]. Figure 10 shows the spectral response at 4.2K measured at different forward biases for a 10-layer (645 Å, boron doped concentration $2\times10^{18}cm^{-3}$ $p^+$ layer and 1290 undoped i layer) p-Si HIWIP sample. The detector shows high responsivity over a wide wavelength range with a peak responsivity of 12.3A/W at 27.5μm, detectivity $D^*$ of $6.6\times10^{10}cmHz^{1/2}W$, and cutoff wavelength of 48μm,

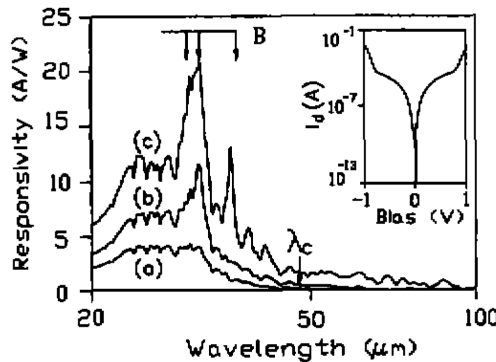


Fig. 10 Spectral response of p-Si HIWIP FIR detector measured at 4.2K under different forward (top positive) bias $V_b$ (a) 0.377V, (b) 0.539V, and (c) 0.791V. The spike responses are associated with excited impurity states with the theoretical energy levels marked by arrows. The other minor features are due to the instrument response function against which the detector output was ratioed. The inset shows the dark current $I_d$ vs $V_b$ of the detector at 4.2K

图 10　不同偏压下 p-Si 探测器的波谱响应，插图为其电流-电压谱

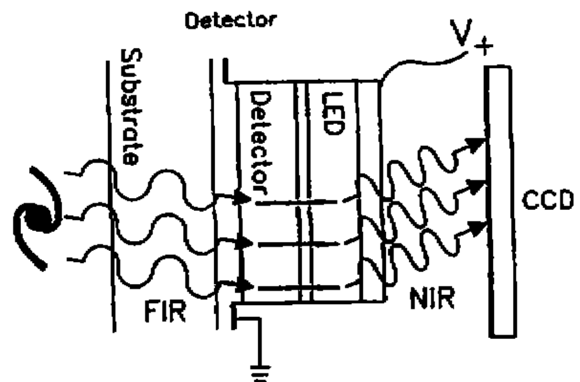


Fig. 11 Schematic of device geometry showing the integrated phtotodiode-LED device with the CCD array for the imaging. Keeping the spatial correlation with the incoming FIR photons, the emitted NIR radiation will form an image in the CCD

图 11　光电探测器与发光二极管集成结构图，发射出的近红外辐射被电荷耦合器件收集

while boron is a substitutional acceptor in silicon with an energy level of 44.4meV(28.0μm).

## 4 DISCUSSION

The preliminary radiation exposure test of the HIWIP detectors shows that they are radiation hard. The detector's gain[12], capacitance characteristics[13], and response time[14] have also been studied in detail. A comparison[8] with Ge:Ga photoconductive detectors suggests that a similar or even better performance may be obtainable. Preliminary results on low doping concentration HIWIP detectors are promising and show that HIWIP detectors have great potentiality to become a strong competitor in FIR applications. It is clear that higher performance and longer $\lambda_c$ (about 200μm or higher) of GaAs and Si HIWIP FIR detectors can be obtained with the emitter layer concentration in the order of $10^{19}cm^{-3}$. It is also possible to design detectors with wider wavelength ranges or to have multicolor detectors by changing the adjacent emitter layer doping concentrations.

Pixelless FIR imager can be made using integrated HIWIP detectors and light emitting diodes (LED), and charge coupled devices (CCD). The idea here is to convert the FIR photons to near IR (NIR) by driving the LED with the photocurrent output of the HIWIP detector so that the imaging can be accomplished by commercial Si CCD cameras, as shown in Fig. 11. In this respect, the photoexcited carriers due to the FIR radiation should trigger the emission of NIR photons from the LED with a high efficiency. A photodiode or a photoconductor connected in series with a LED will be the main device of the up conversion idea. The integrated device consists of a GaAs HIWIP FIR detector, on top of which is grown a shorter wavelenegth InGaAs/GaAs LED.

## ACKNOWLEDGEMENTS

Part of the work was done in Georgia State University, USA. This work was supported in part by the Foundation of Education Administration for Excellent Young Teachers and the National Natural Science Foundation of China. The author would like to acknowledge Drs. Unil Perera, W. J. Schaff, H. C. Liu. M. Buchanan, and S. G. Matsik for their discussion and technical help.

## REFERENCES

[1] HUFFMAN J E, CROUSE A C, HALLECK B L, *et al.* Si:Sb blocked impurity band detectors for infrared astronomy, *J. Appy. Phys.*, 1992, **72**: 273

[2] STACEY G J, BEEMAN J W, HALLER E E, *et al.* Stressed and unstressed Ge:Ga blocked impurity band detectors. *Int. J. Infrared and Millimeter Waves*, 1992, **13**: 1689

[3] BEEMAN J W, HALLER E E. Ge:Ga photoconductor arrays: design considerations and quantitative analysis of prototype single pixels, *Infrared Physics and Technology*, 1994, **35**: 827, and references therein.

[4] LEVINE B F. Quantum well infrared photodetetors, *J. Appl. Phys.*, 1993, **74**: R1.

[5] JAIN S C, ROULSTON D J. A simple expression for band gap narrowing (BGN) in heavily doped Si, Ge, GaAs and $Ge_xSi_{1-x}$ strained layers, *Solid State Electron.*, 1991, **34**: 453

[6] SHEN W Z, PERERA A G U, LIU H C, *et al.* Effect of emitter layer concentration on the performance of GaAs $p^+$-i homojunction far-infrared detectors: a comparison of theory and experiment, *IEEE Trans. Electron Devices*, 1998, **45**: 1671

[7] TOHYAMA S, TERANISHI N, KUNOMA K, *et al.* A new concept silicon homojunction infrared sensor, *IEDM Technical Digest IEEE.*, 1988, **82**

[8] SHEN W Z, PERERA A G U, LIU H C, *et al.* Bias effects in high performance GaAs homojunction far-infrared detectors, *Appl. Phys. Lett.*, 1997, **71**: 2677

[9] STETSON S B, REYNOLDS D B, STAPELBROEK M G, *et al.* Design and performance of block-impurity-band detector focal plane arrays, *Proc. SPIE*, 1986, **686**: 48

[10] SHEN W Z, PERERA A G U, Low frequency noise and interface states in GaAs homojunction far-infrared detectors, *IEEE Trans. Electron Devices.*, 1999, **46**: 811

[11] PERERA A G U, SHEN W Z, LIU H C, *et al.* Demonstration of Si homojunction far-infrared detectors, *Appl. Phys. Lett.*, 1998, **72**: 2307

[12] SHEN W Z, PERERA A G U. Photoconductive generation mechanism and gain in internal photoemission detectors, *J. Appl. Phys.*, 1998, **83**: 3923

[13] PERERA A G U, SHEN W Z, ERSHOV M, *et al.* Negative capacitance in GaAs homojunction far-infrared detectors, *Appl. Phys. Lett.*, 1999, **74**: 3167

[14] SHEN W Z, PERERA A G U. Photoconductivity in homojunction internal photoemission far-infrared detectors, *Infrared Physics and Technology*, 1998, **39**: 329